Supplementary Information

Ground-state electron transfer in all-polymer donor-acceptor blends enables aqueous processing of water-insoluble conjugated polymers

Tiefeng Liu[1,2], Johanna Heimonen[1], Qilun Zhang[1], Chi-Yuan Yang[1,3], Jun-Da Huang[1,3], Han-Yan Wu[1], Marc-Antoine Stoeckel[1,3], Yuxuan Li[4], Sang Young Jeong[5], Adam Marks[6], Xin-Yi Wang[7], Yuttapoom Puttisong[4], Xianjie Liu[1], Silan Zhang[1], Qifan Li[1], Matteo Massetti[1], Weimin M. Chen[4], Han Young Woo[5], Jian Pei[7], Iain McCulloch[6], Feng Gao[4], Mats Fahlman[1], Renee Kroon[1], Simone Fabiano[1,2,3,*]

[1]Laboratory of Organic Electronics, Department of Science and Technology, Linköping University, Norrköping SE-60174, Sweden.
[2]Wallenberg Initiative Materials Science for Sustainability, Department of Science and Technology, Linköping University, Norrköping SE-60174, Sweden.
[3]n-Ink AB, Teknikringen 7, SE-583 30 Linköping, Sweden.
[4]Electronic and Photonic Materials, Department of Physics, Chemistry, and Biology, Linköping University, Linköping SE-58183, Sweden.
[5]Department of Chemistry, College of Science, Korea University,136-713 Seoul, Republic of Korea.
[6]Department of Chemistry, University of Oxford, Oxford OX1 3TA, UK.
[7]Beijing National Laboratory for Molecular Sciences (BNLMS), Key Laboratory of Polymer Chemistry and Physics of Ministry of Education, Center of Soft Matter Science and Engineering, College of Chemistry and Molecular Engineering, Peking University, Beijing 100871, China.

Correspondence should be addressed to: simone.fabiano@liu.se

Synthesis of PCAT-K

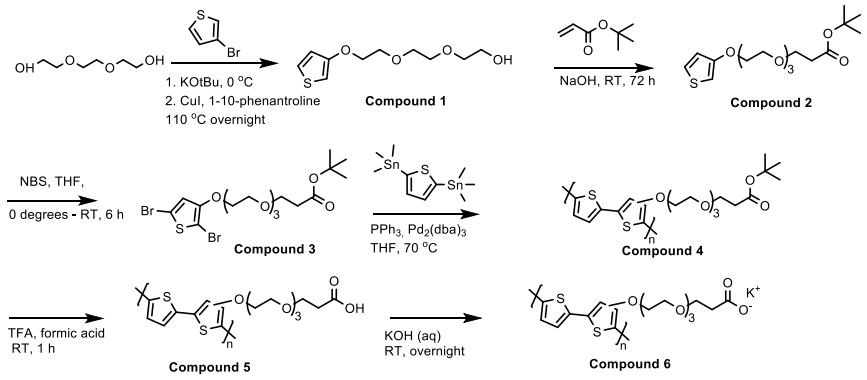

Compound 1

Ullman aryl ether synthesis

7.05 g (mmol, 7.5 eq) triethylene glycol was added to a 25 ml roundbottom flask and lowered into a 0 °C ice bath under nitrogen atmosphere. 1.03 g potassium tertbutoxide was added in portions and the mixture was stirred for 10 minutes. The vessel was transferred to a RT oil bath and stirred for 50 minutes. The bath temperature was increased to 50 °C for 10 min. 55 mg (0.61 mmol, 0.1 eq) CuI was added along with 220.4 mg 1,10-phenantroline and 0.57 ml (1 g, 6.1 mmol, 1 eq) of 3-bromothiophene. The mixture was stirred at 110 °C overnight. The reaction mixture was transferred to a 500 ml roundbottom flask and the vessel was washed with some MeOH. 50 ml of silica gel was added with diethyl ether to form a slurry. The solvents were carefully evaporated, and the sample was dried in vacuo for 1.5 h. The product was purified on a silica gel column prepared with diethyl ether and eluted with 5 % MeOH in diethyl ether. Fractions containing the product were combined, the solvent evaporated, and the product was stored in the fridge. The final yield was 0,88 g (62 %). ($_1$H NMR (500 MHz, cdcl$_3$) δ 7.16 (dd, *J* = 5.3, 3.1 Hz, 1H), 6.78 (dd, *J* = 5.2, 1.5 Hz, 1H), 6.26 (dd, *J* = 3.2, 1.6 Hz, 1H), 4.12 (dd, *J* = 5.7, 3.8 Hz, 2H), 3.89 – 3.79 (m, 2H), 3.70 (dddd, *J* = 14.0, 8.3, 6.0, 4.3 Hz, 7H), 3.64 – 3.58 (m, 2H)), ($_{13}$C NMR (126 MHz, cdcl3) δ 157.82, 125.02, 119.88, 97.91, 72.79, 71.09, 70.69, 70.01, 69.83, 62.07.)

Compound 2

Oxa-Michael addition

653.4 mg (2.8 mmol, 1 eq) of compound I was combined with 451.5 mg (3.5 mmol, 1.3 eq) of tert-butyl acrylate and 8 mg of NaOH in a 10 ml roundbottom flask. The sample was covered from light and stirred at RT for 72 h. The product was purified on a silica gel column and eluted with 25 % acetone in petroleum ether. The solvent was removed and the product was dried in vacuo overnight, the final yield was 0,95 g (94 %). ($_1$H NMR (500 MHz, cdcl$_3$) δ 7.16 (dd, *J* = 5.2, 3.1 Hz, 1H), 6.77 (dd, *J* = 5.2, 1.6 Hz, 1H), 6.26 (dd, *J* = 3.1, 1.5 Hz, 1H), 4.13 – 4.09 (m, 2H), 3.87 – 3.81 (m, 2H), 3.75 – 3.57 (m, 10H), 2.50 (t, *J* = 6.6 Hz, 2H), 1.44 (s, 9H)), ($_{13}$C NMR (126 MHz, cdcl$_3$) δ 171.23, 157.95, 124.95, 119.93, 97.85, 80.83, 77.61, 77.36, 77.10, 71.14, 70.99, 70.90, 70.71, 70.03, 69.92, 67.24, 36.61, 28.43.) 26

Compound 3

Bromination

In a typical procedure, 0.5072 g (1.41 mmol, 1 eq) of compound 2 was combined with 10 ml of tetrahydrofuran, in a 25 ml round bottom flask, under nitrogen atmosphere, and degassed for 30 minutes. The solution was allowed to cool to 0 °C for 15 minutes before 0.50 g (2.82 mmol, 2 eq) of N-bromo succinimide was added portion wise. The mixture was reacted for 1.5 h at 0 °C and was then allowed to react overnight at RT. After 5 h, an additional portion of N-bromo succinimide was added to drive the reaction to completion. The reaction was neutralized by addition of 5 ml 1 M sodium bicarbonate and

stirred for 15 min. The solution was transferred to an extraction flask along with 140 ml of diethyl ether. The organic phase was extracted with 1x50 ml of 1 M sodium bicarbonate and 3x50 ml of brine. The water phase was extracted with 2x50 ml of diethyl ether. The organic phases were combined and dried over sodium sulphate and magnesium sulphate. The solvent was removed by evaporation and the product was dried in vacuo overnight. The product was purified on a silica gel column and eluted with 20 % acetone in petroleum ether. The eluate was collected in fractions and monitored by TLC. The final yield was 0.35 g (45 %) of pure product which was collected as a yellow oil. (1H NMR (500 MHz, cdcl3) δ 6.82 (s, 1H), 4.17 – 4.13 (m, 2H), 3.81 – 3.76 (m, 2H), 3.74 – 3.68 (m, 4H), 3.67 – 3.59 (m, 6H), 2.50 (t, J = 6.6 Hz, 2H), 1.44 (s, 9H)), (13C NMR (126 MHz, cdcl3) δ 171.25, 154.09, 121.85, 109.93, 72.39, 71.34, 71.02, 70.93, 70.75, 70.17, 67.26, 36.63, 28.45.)

Compound 4

Stille Coupling

A dried 50 mL round bottom flask was charged with compound 4 (2 g, 3.86 mmol) and 2,5-bis(trimethylstannyl)thiophene (1.58 g, 3.86 mmol, 1.0 eq) and dissolved in dry, sparged (30 min with N_2) tetrahydrofuran (250 mL). Then, tris(dibenzylideneacetone)dipalladium(0) (77.2 mg, 2 mol-%), triphenylphosphine (83 mg, 8 mol-%) were added under nitrogen atmosphere. After dissolving, the solution was heated to 70 °C under stirring, during which the color progressed to deep red and the viscosity increased. After 48 hours reaction time, the solution was cooled to room temperature and poured into hexanes under vigorous stirring which yielded blue fibers. After filtration, the polymer was redissolved in chlofororm and vigorously stirred with a 5% m/v solution of sodium diethyldithiocarbamate trihydrate in deionized water at reflux under N_2. After liquid-liquid extraction, the chloroform solution was reduced in volume, precipitated in heptane and transferred to a Soxhlet extraction thimble. Then the polymer was Soxhlet extracted with heptane until each washing yielded a clear extract. After collecton with isopropanol and drying the polymer solution *in vacuo*, the polymer was precipitated in isopropanol, dried under vacuum to yield 1.34 grams (82%) of the target material as a blue sticky material. (1H-NMR (500 MHz, cdcl3) δ 7.5-6.83 (m, 3H), 4.39-4.22 (m, 2H), 3.97-3.85 (m, 2H), 3.80-3.40 (m, 10H), 2.55-2.35 (m, 2H), 1.49-1.28 (2, 9H)).

Compound 5 and 6

Acid catalyzed deprotection and formation of the polyanion

1 g of compound 4 was dissolved in a sparged mixture of 15 ml of formic acid and 4 ml of trifluoroacetic acid before being stirred overnight at room temperature under nitrogen atmosphere. The polymer was precipitated in water and centrifuged at 3500 rpm for 10 min. The supernatant was discarded, and the pellet was washed with additional water 3 times before the product was collected. Compound 5 is an insoluble dark purple solid, the yield of compound 5 was not determined. Compound 5 was added to a round bottom flask along with 150 ml of water and 1 g of potassium hydroxide forming a purple viscous solution which was stirred at 45 °C overnight. The polymer was precipitated in acetone giving dark purple particles that were collected via centrifugation. The particles were successively washed with acetone:water mixture (90:10) to remove excess potassium hydroxide and collected. This process yielded 0,993 g (quantitative) of a dark purple solid.

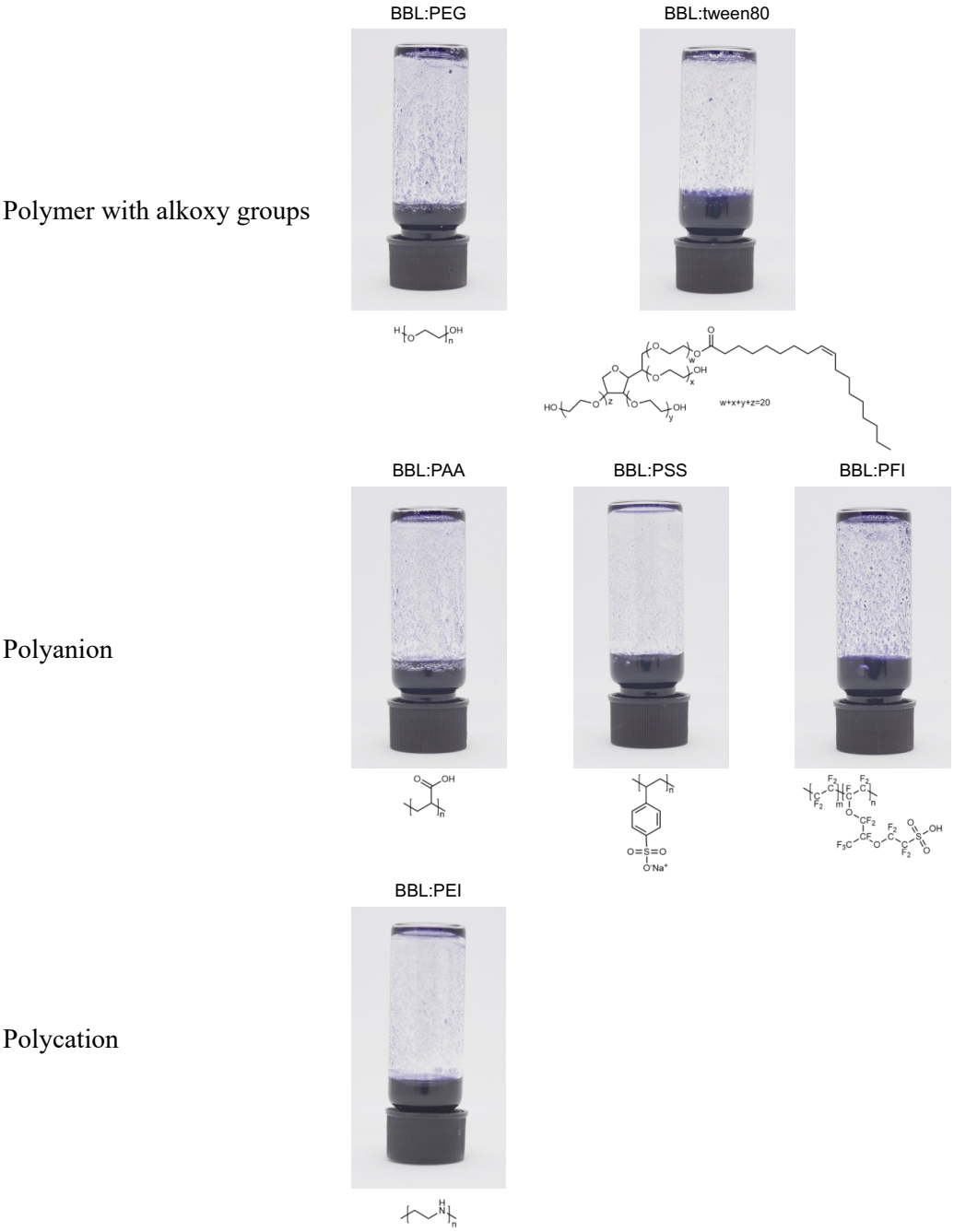

Supplementary Figure 1. Pictures of BBL dispersion in water in the presence of common surfactants: Poly(ethylene glycol) (PEG). Polyethylene glycol sorbitan monooleate (TWEEN 80). Poly(acrylic acid) (PAA). Poly(sodium-4-styrene sulfonate) (PSS). Perfluorinated sulfonic acid ionomers (PFI). Linear poly(ethyleneimine) (PEI). For all surfactants, the BBL:surfactant ratio is 1:1 and the total concentration is 2 mg/ml in water. The surfactant chemical structures are presented below the pictures.

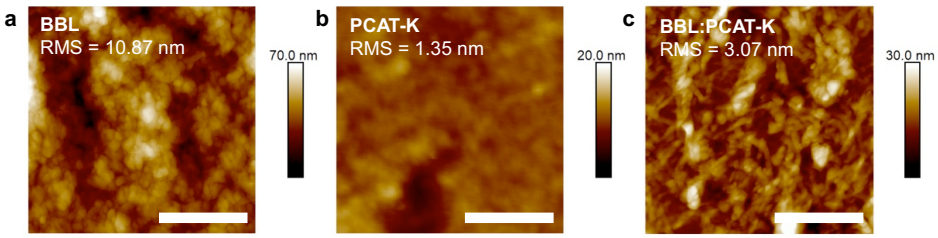

Supplementary Figure 2. Atomic force microscope (AFM) images of (a) BBL, (b) PCAT-K, and (c) BBL:PCAT-K films on a glass substrate. The scale bar is 400 nm.

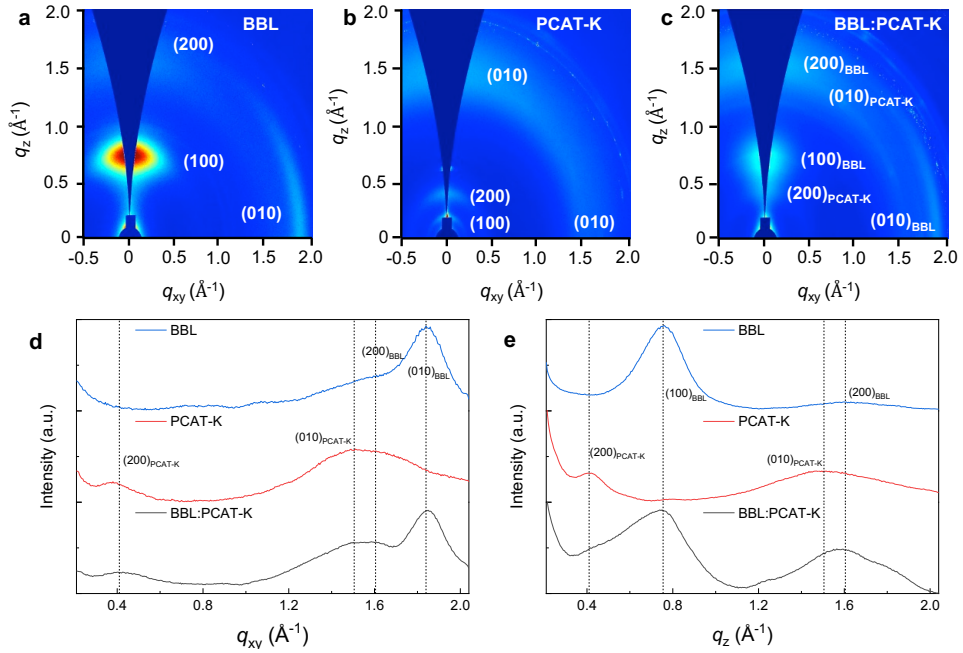

Supplementary Figure 3. 2D GIWAXS patterns of (a) BBL, (b) PCAT-K, and (c) BBL:PCAT-K. Out-of-plane (d) and in-plane (e) GIWAXS line cuts of BBL, PCAT-K, and BBL:PCAT-K films. The mass ratio of BBL and PCAT-K is 1:1.

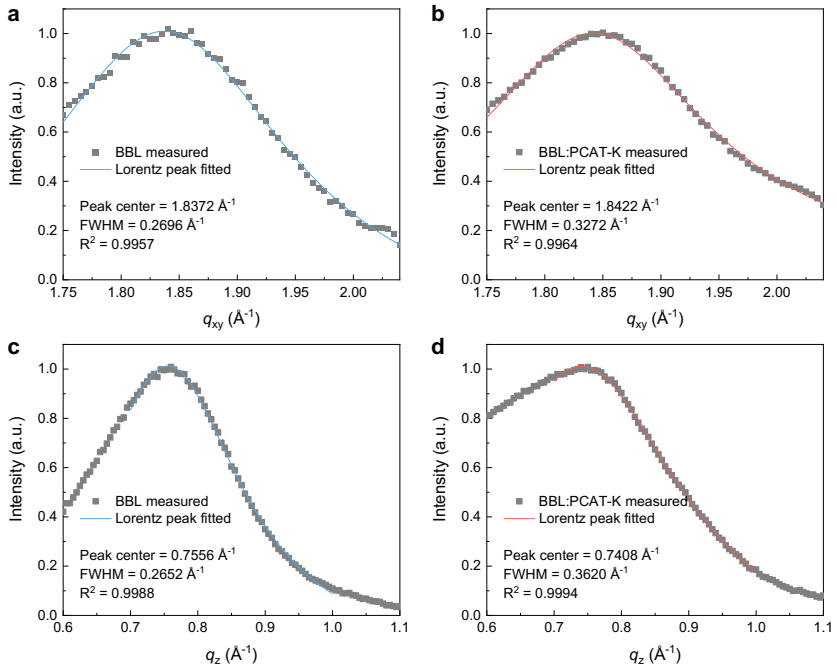

Supplementary Figure 4. π-π stacking (010) diffraction analysis of (a) BBL and (b) BBL:PCAT-K. Lamellar (100) diffraction analysis of (c) BBL and (d) BBL:PCAT-K.

Pristine BBL presented a predominant edge-on orientation on the substrate, with a strong lamellar (100) peak at q_z = 0.756 Å^{-1} (d-spacing= 8.32 Å) and a strong π-π stacking (010) peak at q_{xy} = 1.837 Å^{-1} (d-spacing = 3.42 Å) while the PCAT-K shows a mixed edge-on and face-on orientation. On the contrary, the BBL:PCAT-K blend film shows a weak diffraction pattern. From the linecuts, the diffraction peaks relative to BBL and PCAT-K can be observed in the blend film with the weak intensity and broad width, indicative of a good intermixing between the two polymers and a poor aggregation. Particularly, the coherence lengths of BBL π-π stacking and lamellar packing in the blend film decrease from 20.98 Å to 17.28 Å and 21.32 Å to 15.62 Å, respectively.

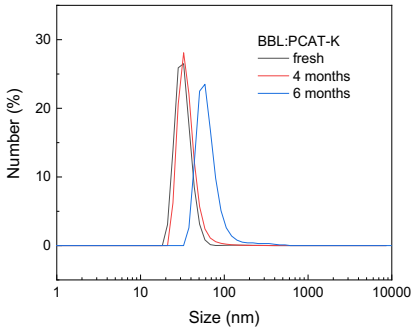

Supplementary Figure 5. Particle size distribution of BBL:PCAT-K stored in ambient condition.

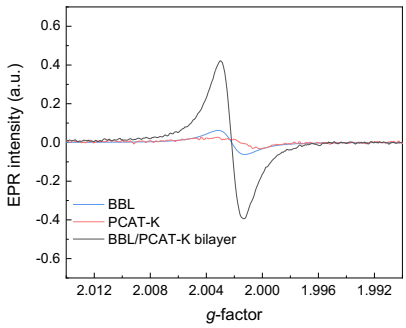

Supplementary Figure 6. EPR signals of BBL, PCAT-K, and BBL/PCAT-K bilayer films.

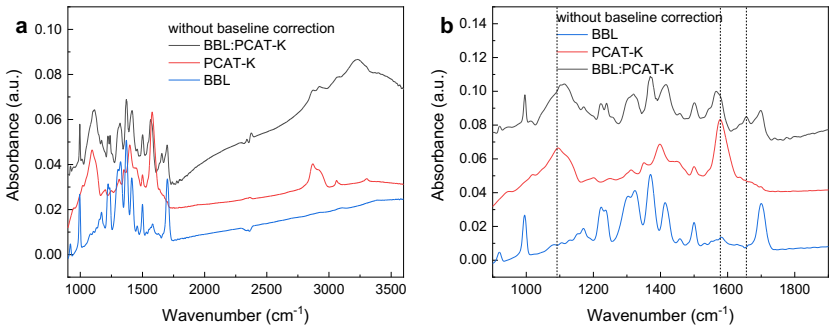

Supplementary Figure 7. Raw unnormalized FTIR absorption spectra of BBL, PCAT-K, and BBL:PCAT-K films. (a) A broad absorption band in the range 2000-3500 cm^{-1} is visible for BBL:PCAT-K film and can be attributed to polarons[1]. (b) A new peak at 1655 cm^{-1}, assigned to antisymmetric C=O stretching, appears in the FTIR spectrum of BBL:PCAT-K. This is the fingerprint of negative polarons in BBL[2]. The peak at 1578 cm^{-1}, assigned to the antisymmetric $C_\alpha = C_\beta$ bonds stretching of PCAT, shifts to lower wavenumbers, indicating doping of PCAT-K[3].

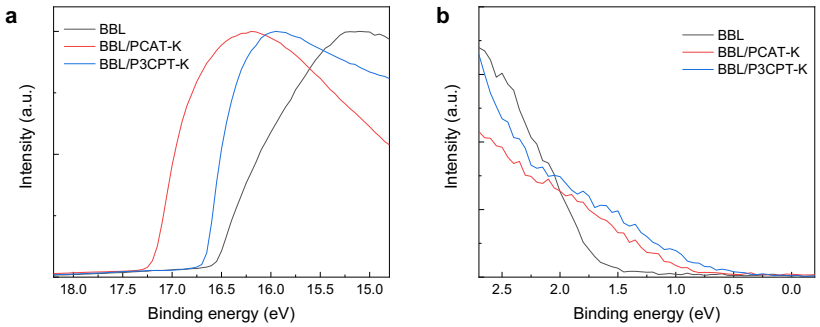

Supplementary Figure 8. UPS spectra of BBL (black), BBL/PCAT-K (red), and BBL/P3CPT-K (blue) films. The left panel shows the secondary electron cut-off region, and the right panel shows the frontier valence region. The starting substrate is gold for all cases. The work function (WF) can be determined from the secondary electron cut-off and is 4.63 eV for the BBL films. When PCAT-K and P3CPT-K are deposited onto BBL to form bilayer structures, the chemical potential is equilibrated across the bilayers. If electron transfer occurs in this process, a shift of the secondary electron cut-off is generated in the UPS spectra that signifies a corresponding shift of the vacuum level at the interface. The PCAT-K film shows a large shift in the secondary electron cut-off when deposited on top of the BBL film, which is in agreement with substantial electron transfer from PCAT-K to BBL. Only a near-negligible shift in the secondary electron cut-off is seen for P3CPT-K on BBL, suggesting an absence of significant GSET.

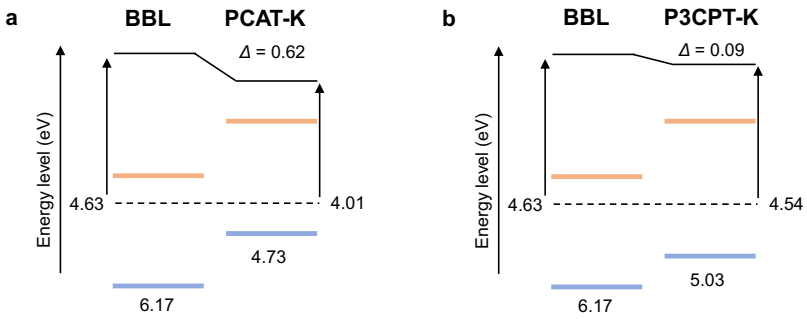

Supplementary Figure 9. The resulting down-shift (Δ, in eV) of the vacuum level for BBL/PCAT-K and BBL/P3CPT-K heterojunctions is reported in the diagram.

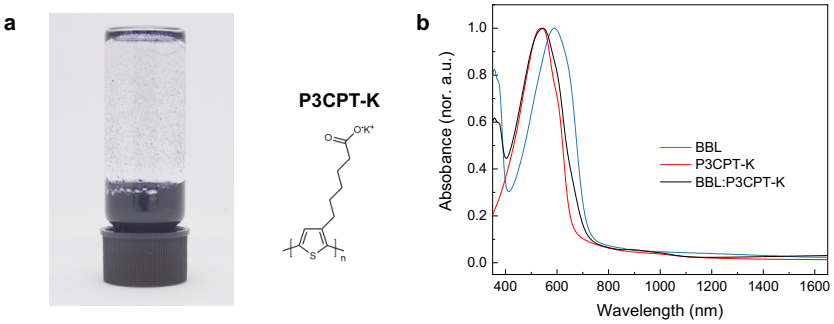

Supplementary Figure 10. (a) Photograph of BBL:P3CPT-K dispersion. The BBL:P3CPT-K ratio is 1:1. The chemistry structure of P3CPT-K is presented on the right. (b) The absorbance of BBL, P3CPT-K, and BBL:P3CPT-K film. The absorbance was normalized to the maximum value.

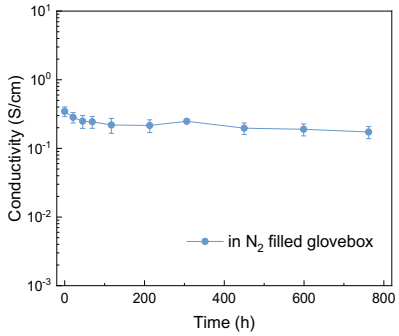

Supplementary Figure 11. Evolution of the electrical conductivity of BBL:PCAT-K film stored in an N_2-filled glovebox. Error bars indicate the SD of ten experimental replicates.

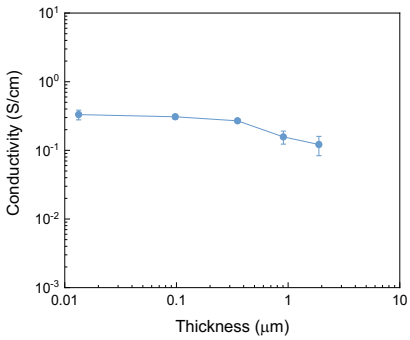

Supplementary Figure 12. Thickness-dependence of the conductivity of BBL:PCAT-K film. The thin film (< 100 nm) was deposited by spin-coating while the thick film (> 100 nm) was deposited by drop-casting. Error bars indicate the SD of ten experimental replicates.

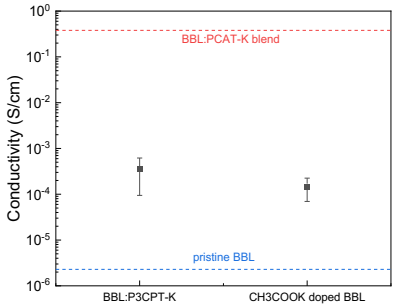

Supplementary Figure 13. The conductivity of BBL:P3CPT-K and potassium acetate-doped BBL.

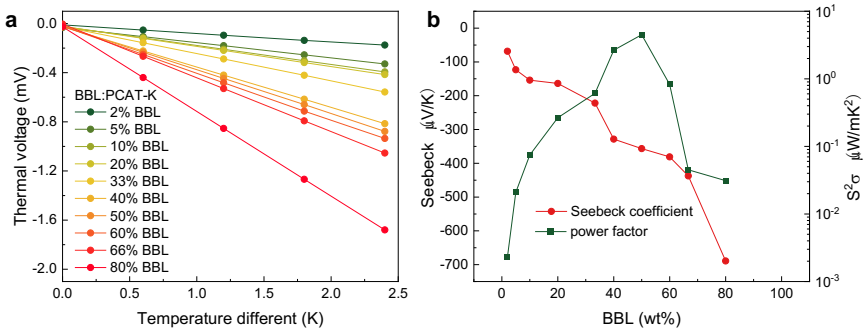

Supplementary Figure 14. (a) Temperature difference dependent thermal voltage of BBL:PCAT-K films with different BBL content. (b) Seebeck coefficient and power factor of BBL:PCAT-K films with different BBL content.

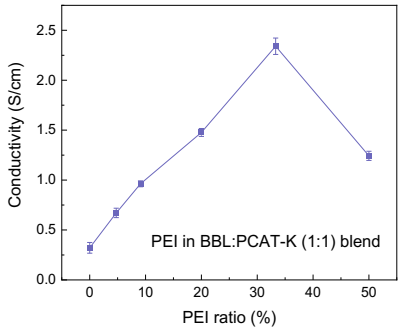

Supplementary Figure 15. Conductivity of BBL:PCAT-K films at different content of PEI. Error bars indicate the SD of ten experimental replicates.

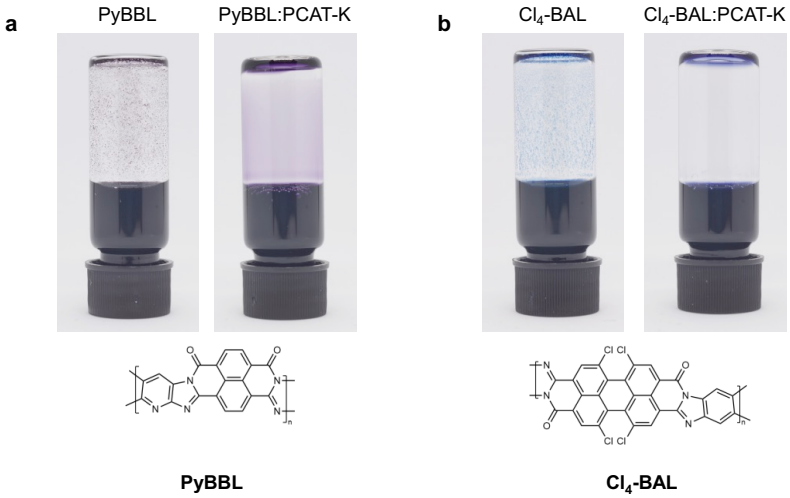

Supplementary Figure 16. (a) Photographs of PyBBL (1 mg/ml) and PyBBL:PCAT-K 1:1.5 (2.5 mg/ml) aqueous solutions. (b) Photographs of Cl_4-BAL (1 mg/ml) and Cl_4-BAL:PCAT-K 1:1 (2 mg/ml) aqueous solutions. The PyBBL and Cl_4-BAL water dispersions were prepared using the same solvent-exchange method used for BBL.

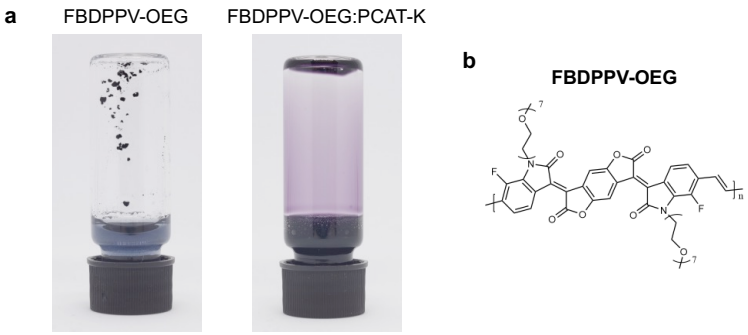

Supplementary Figure 17. Photographs of FBDPPV-OEG (10 mg/ml) and FBDPPV-OEG:PCAT-K 1:1 (20 mg/ml) aqueous solutions (a) and chemical structure of FBDPPV-OEG in (b).

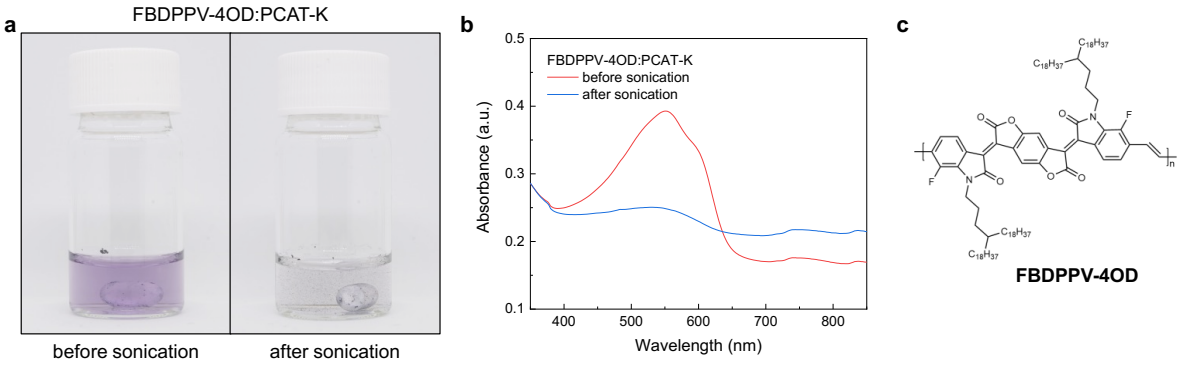

Supplementary Figure 18. (a) Photographs of FBDPPV-4OD:PCAT-K 1:1 (0.1 mg/ml) solution before and after 5 min of sonication. (b) Absorbance spectrum of their corresponding solution, showing the disappearance of PCAT-K from solution after sonication. (c) Chemical structure of FBDPPV-4OD.

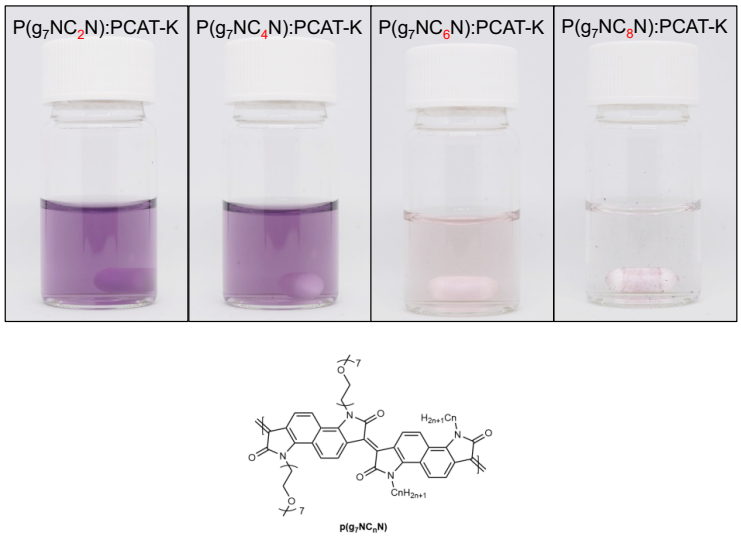

Supplementary Figure 19. Photographs of P(g_7NC_nN):PCAT-K (1:1) aqueous solutions. P(g_7NC_nN) has polar side chains and alkyl side chains with gradually increasing lengths (from C_2 to C_8). P(g_7NC_nN) with short alkyl side chains, like P(g_7NC_2N) and P(g_7NC_4N), can dissolve in water in the presence of PCAT-K, while P(g_7NC_nN) with long alkyl side chain, like P(g_7NC_6N) and P(g_7NC_8N), trap PCAT-K out of the aqueous solution. For all P(g_7NC_nN):PCAT-K blends, the concentrates was 0.1 mg/ml.

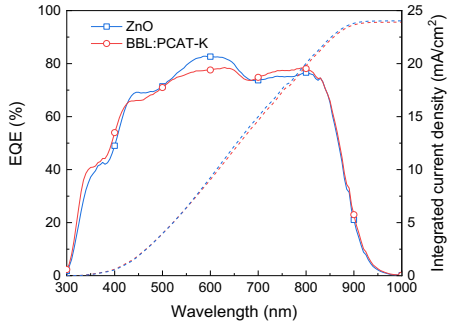

Supplementary Figure 20. EQE spectra of the inverted ITO/ETL/PM6:Y6:$PC_{71}BM$/MoO_3/Ag, where ETL is BBL:PCAT-K or ZnO as reference. The integrated current density is 23.91 and 24.03 mA cm^{-2} for BBL:PCAT-K and ZnO based devices respectively, which is close to the value obtained from the *J-V* curves.

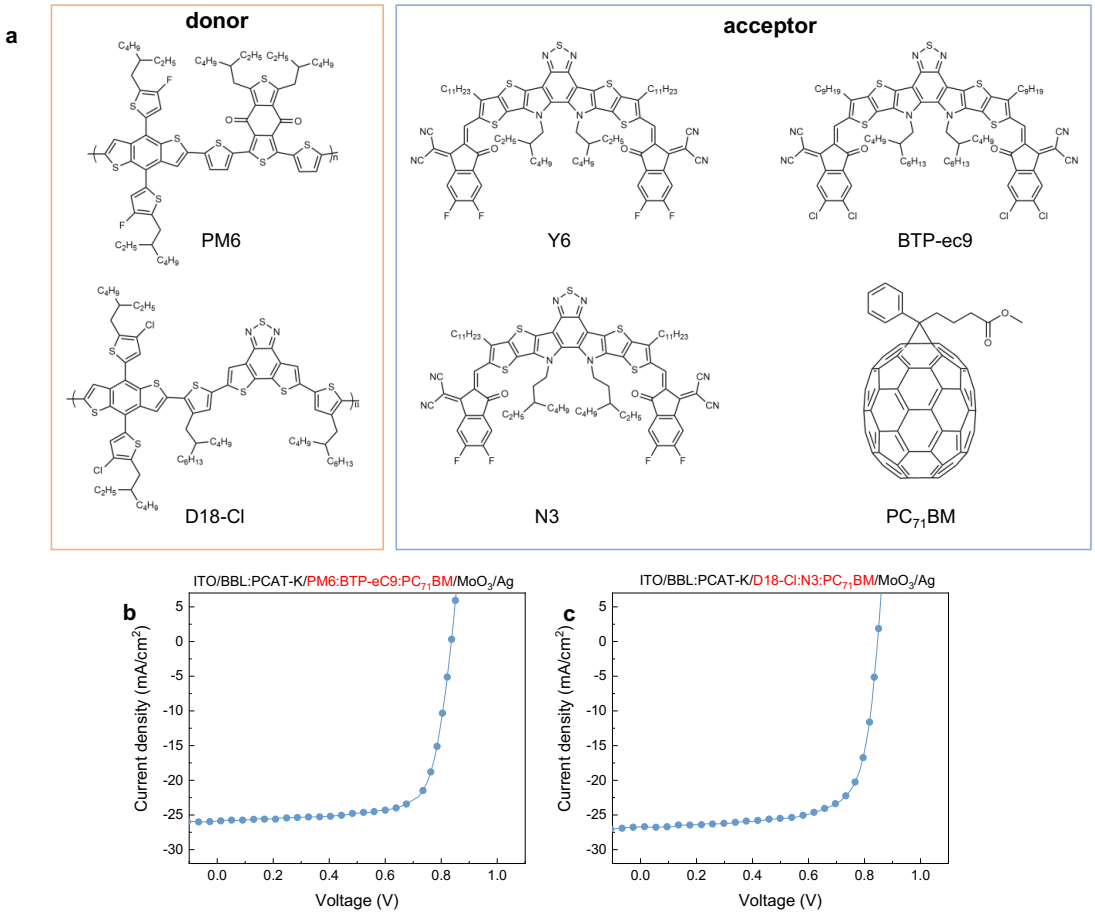

Supplementary Figure 21. (a) Chemical structure of the organic active materials used in this work. The *J-V* curves of OSCs with the inverted structure ITO/BBL:PCAT-K/active layer/MoO_3/Ag, where the active layer is (b) PM6:BTP-ec9:$PC_{71}BM$ or (c) D18-Cl:N3:$PC_{71}BM$.

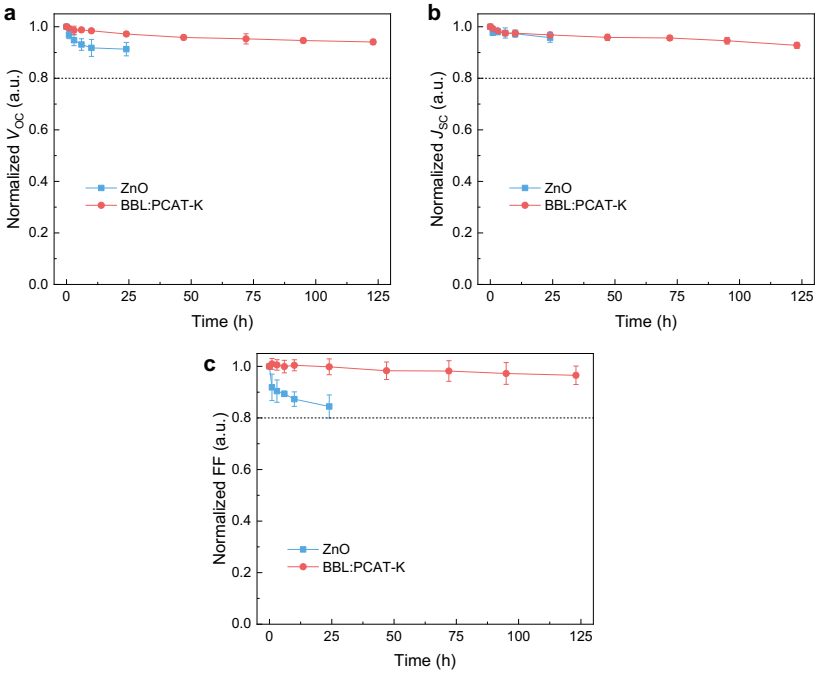

Supplementary Figure 22. Normalized (a) V_{OC}, (b) J_{SC}, and (c) FF of OSCs with the inverted structure ITO/ETL/PM6:Y6:$PC_{71}BM$/MoO_3/Ag, where ETL is either BBL:PCAT-K or ZnO, as a function of the illumination time under 100 mW cm^{-2} in an N_2-filled glovebox. Error bars indicate the SD of eight experimental replicates.

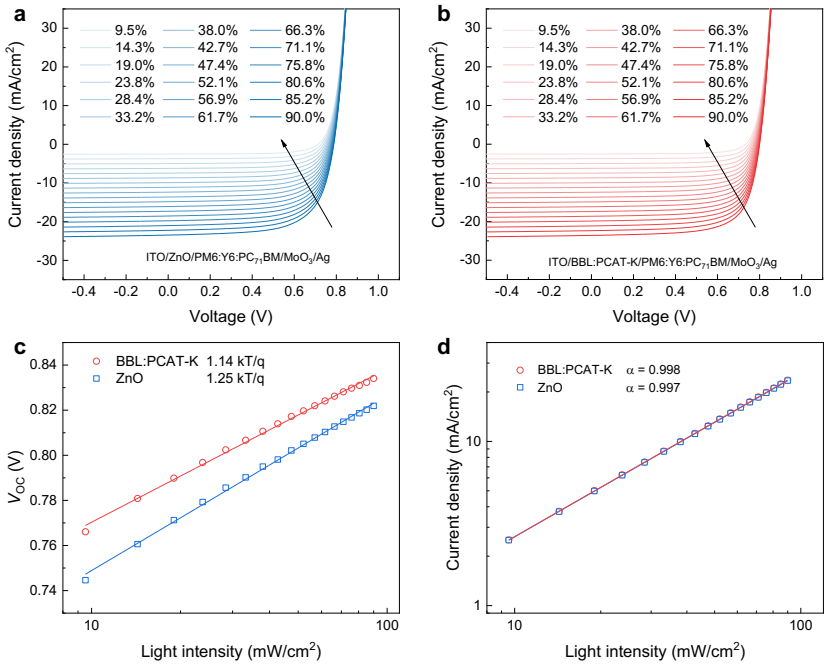

Supplementary Figure 23. *J-V* curves of OSCs with the inverted structure of ITO/ETL/PM6:Y6:$PC_{71}BM$/MoO_3/Ag, where ETL is (a) ZnO as reference or (b) BBL:PCAT-K. The relationship between (c) V_{OC} or (d) J_{SC} verse light intensity extracted from *J-V* curves. The exponent α of the equation $J_{SC} \propto P^{\alpha}$ is close to 1 (0.998 for BBL:PCAT-K as ETL and 0.997 for ZnO as ETL), indicating negligible bimolecular recombination and that all carriers can be collected by the electrodes[4]. However, the slope of V_{OC} versus ln(*P*) in BBL:PCAT-K-based devices is smaller than that of ZnO-based reference device (1.14 k*T*/q vs 1.25 k*T*/q, where k is the Boltzmann constant, *T* is the absolute temperature and q is the elementary charge), suggesting suppression of trap-assisted recombination[5].

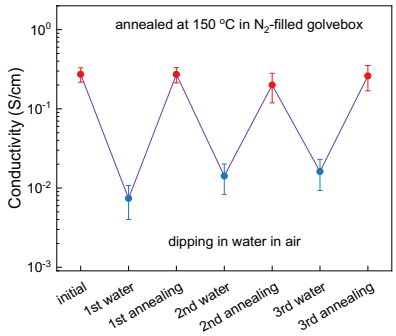

Supplementary Figure 24. Conductivity of BBL:PCAT-K (1:1) film dipped in water for 1 min and annealed in an N_2-filled glovebox. Error bars indicate the SD of ten samples. The reversible conductivity upon water/annealing treatment indicates that the decrease in conductivity is due to trapping/de-trapping of charges by water or oxygen[6].

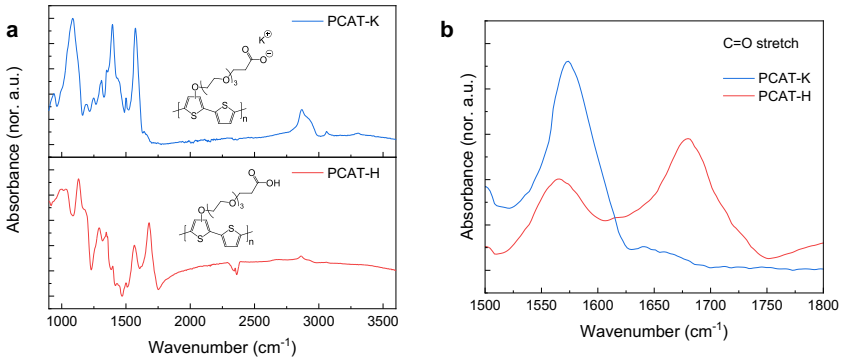

Supplementary Figure 25. FT-IR spectra of PCAT-K converting from the salt form to the acid form (PCAT-H) upon treatment with citric acid (10 mg/ml in IPA). The carboxylic acid functionalized PCAT-H is water-insoluble[7,8].

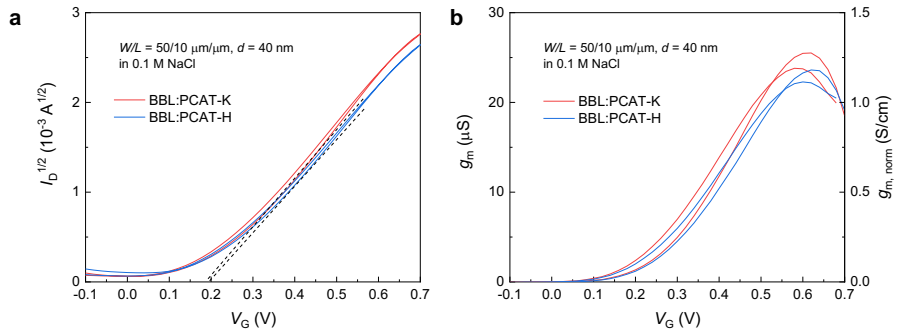

Supplementary Figure 26. (a) Threshold voltages and (b) normalized transconductance of BBL:PCAT-K and crosslinked BBL:PCAT-H based OECTs. The OECT's channel geometry is W = 50 μm, L = 10 μm, d = 40 nm.

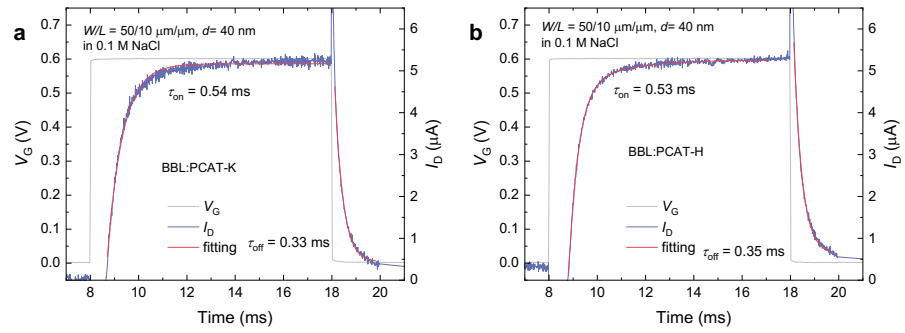

Supplementary Figure 27. Transient response of (a) BBL:PCAT-K and (b) crosslinked BBL:PCAT-H based OECTs. The OECT's channel geometry is W = 50 μm, L = 10 μm, d = 40 nm.

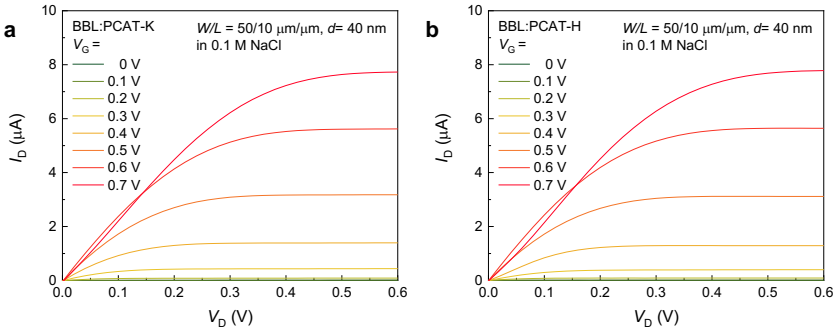

Supplementary Figure 28. Output curves of (a) BBL:PCAT-K and (b) crosslinked BBL:PCAT-H based OECTs. The OECT's channel geometry is W = 50 μm, L = 10 μm, d = 40 nm.

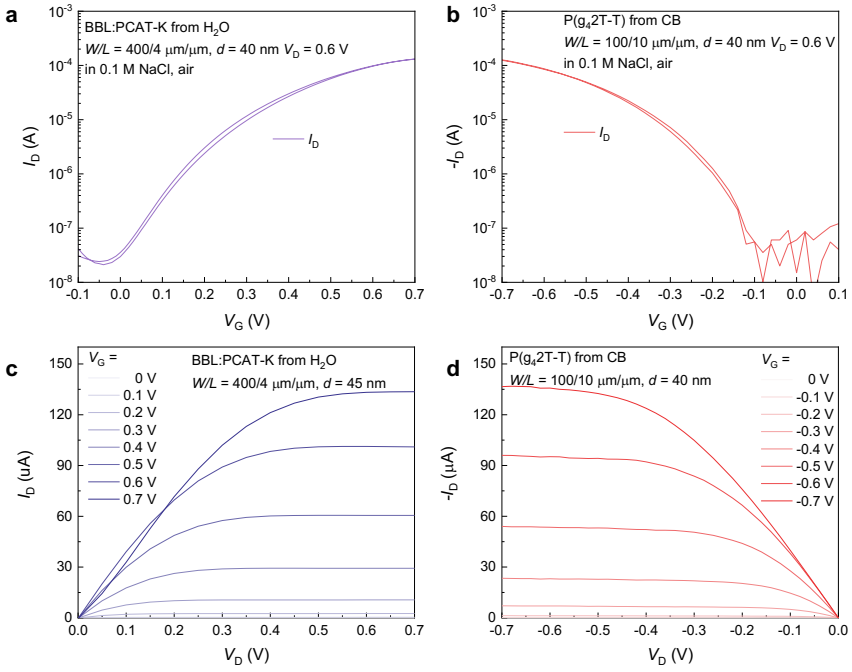

Supplementary Figure 29. Transfer curves of n-type BBL:PCAT-K (a) and p-type P(g42T-T) (b) based OECTs and output curves of n-type BBL:PCAT-K (c) and p-type P($g_4$2T-T) (d) based OECTs. The OECT's channel geometry is W/L = 400/4 μm/μm for n-type OECT and W/L = 100/10 μm/μm for p-type OECT, respectively, while the thickness of both BBL:PCAT-K and P($g_4$2T-T) film is about 40 nm.

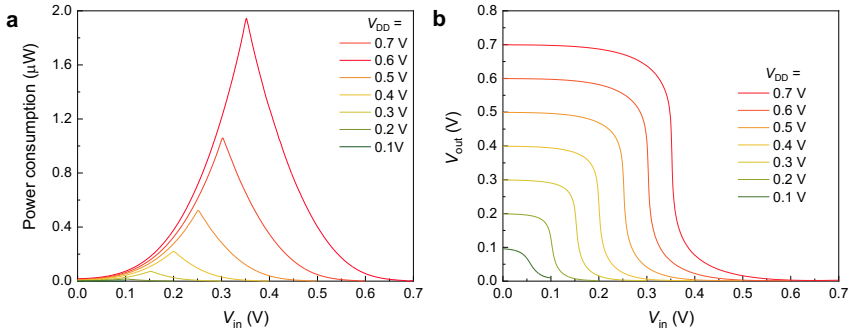

Supplementary Figure 30. (a) Power consumption and (b) voltage output of the complementary inverter at various supply voltages.

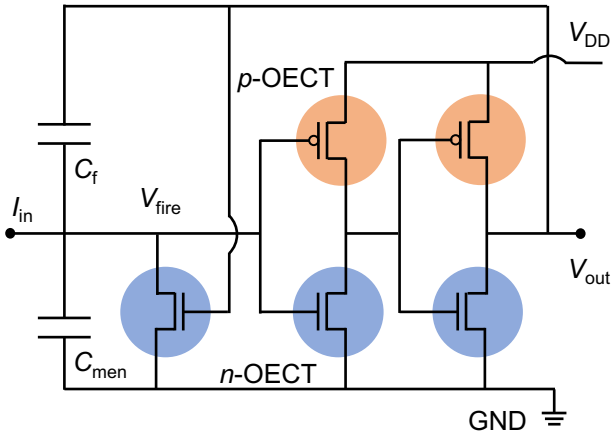

Supplementary Figure 31. Circuit of the integrate and fire type organic electrochemical neuron.

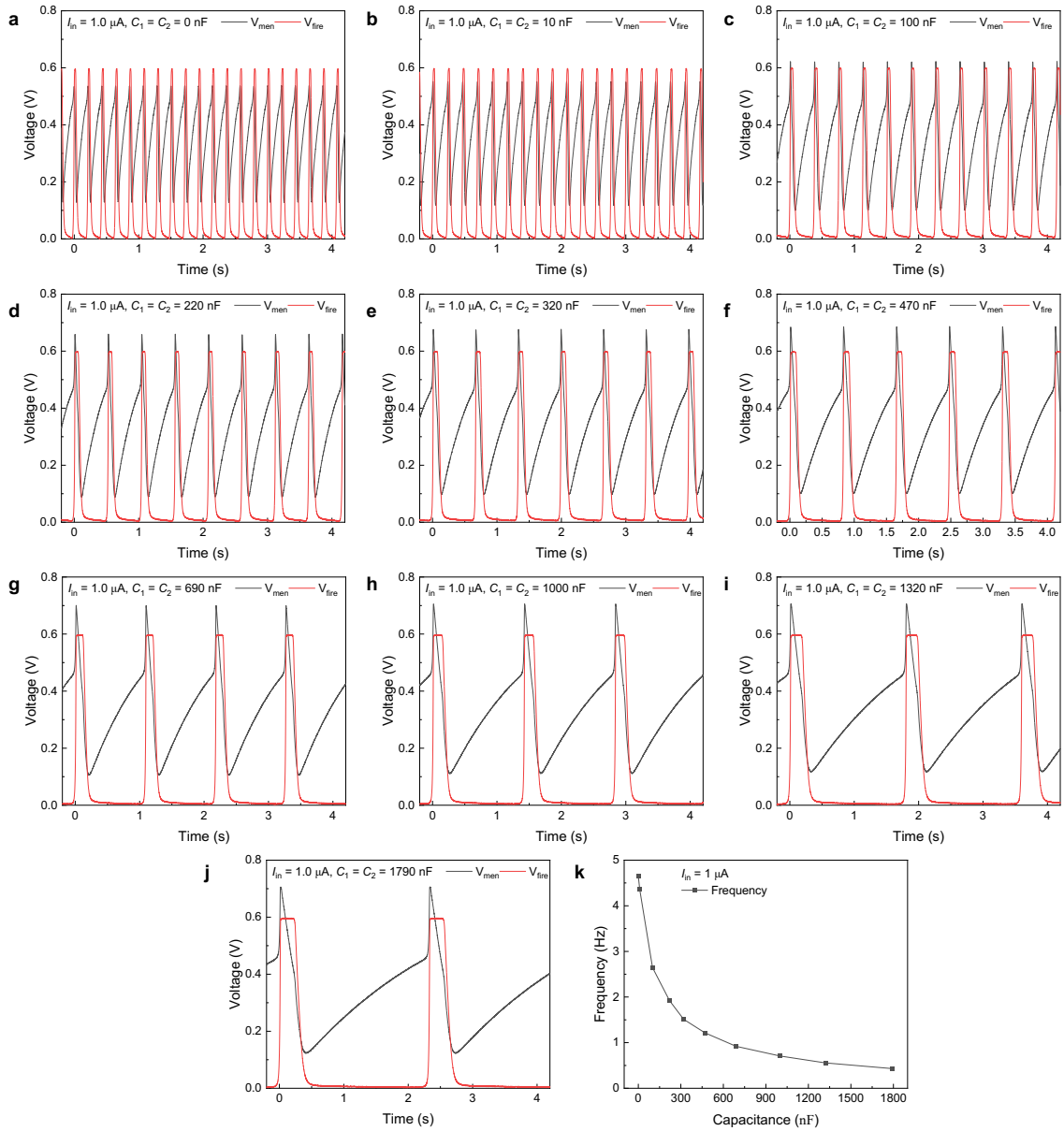

Supplementary Figure 32. Neuron characteristics at various capacitance values and a constant input current of 1 μA.

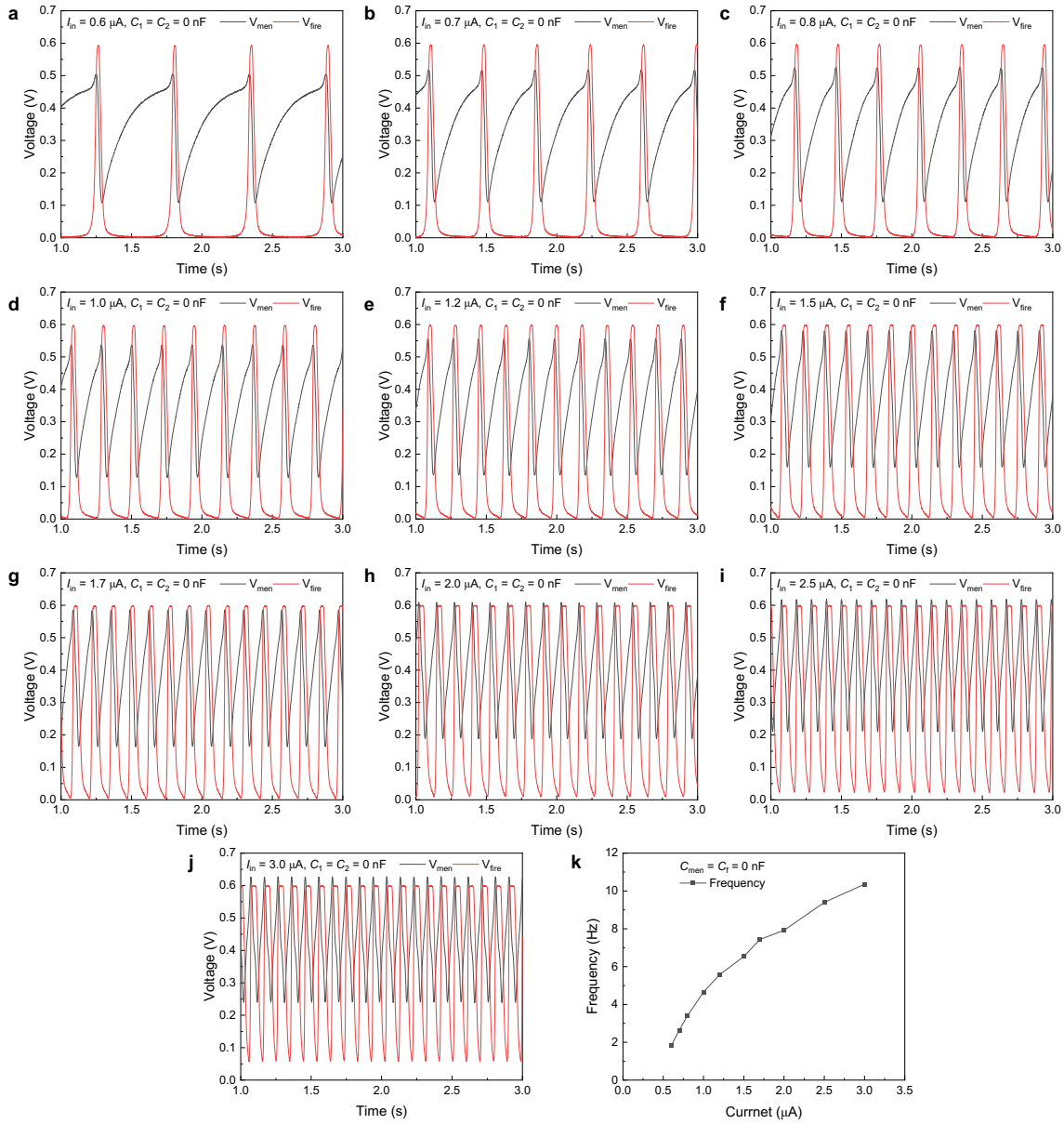

Supplement Figure 33. Neuron's characteristics at various input currents and a constant capacitor C_{men} and C_{f} of 0 nF.

Supplementary Table 1. Absolute spin counts and spin densities in the pristine BBL, PCAT-K films, BBL:PCAT-K blend film, and BBL/PCAT-K bilayers as measured by EPR spectroscopy.

film	Abs. spin ($\times 10^{14}$ counts)	Volume ($\times 10^{-3}$ mm^{-3})	Spin density ($\times 10^{19}$ cm^{-3})
BBL	0.44	39.57	0.11
PCAT-K	0.51	11.25	0.45
BBL/PCAT-K (bilayer)	2.52	N.A.	N.A.
BBL:PCAT-K (blend)	9.21	41.40	2.23

Supplementary Table 2. Photovoltaic parameters of inverted OSCs with structure ITO/ETL/active layer/MoO_3/Ag measured under 100 mW cm^{-2} AM 1.5 G illumination. Average value and standard deviation data are calculated from 16 devices. The value in the brackets is extracted from the device with the best efficiency.

Active layer	ETL	V_{OC} (V)	J_{SC} (mA cm^{-2})	FF	PCE (%)
PM6:Y6:$PC_{71}BM$	ZnO	0.82 ± 0.01 (0.83)	25.36 ± 0.41 (25.85)	0.70 ± 0.02 (0.72)	14.67 ± 0.56 (15.44)
	BBL:PCAT-K	0.83 ± 0.01 (0.84)	25.27 ± 0.45 (25.78)	0.71 ± 0.02 (0.74)	15.38 ± 0.61 (16.03)
PM6:BTP-ec9:$PC_{71}BM$	BBL:PCAT-K	0.83 ± 0.01 (0.84)	25.73 ± 0.27 (25.92)	0.71 ± 0.02 (0.74)	15.48 ± 0.48 (16.11)
D18-Cl:N3:$PC_{71}BM$	BBL:PCAT-K	0.84 ± 0.01 (0.85)	26.58 ± 0.25 (26.72)	0.71 ± 0.02 (0.73)	15.86 ± 0.60 (16.58)

Supplementary Table 3. Summary of the characteristics of BBL:PCAT-K-based OECTs. The OECT's channel geometry is W = 50 μm, L = 10 μm, d = 40 nm.

Materials	Solvent	V_{th} (V)	$g_{m,norm}$ (S/cm)	τ_{ON} (ms)	τ_{OFF} (ms)	I_{ON}/I_{OFF}
BBL:PCAT-K	Water	0.19	1.28	0.54	0.33	1.9×10^3
BBL:PCAT-H	Water	0.20	1.18	0.53	0.35	1.6×10^3

Supplementary Table 4. Performance of OECT-based complementary inverters.

V_{DD} (V)	V_M (V)	Gain (V/V)	V_{IL} (V)	V_{IH} (V)	NM_L (V)	NM_H (V)	NM (%)	P_{static} (nW)	$P_{dynamic}$ (μW)
0.7	0.353	54.8	0.298	0.412	0.298	0.288	83.7	18.3	1.94
0.6	0.303	42.7	0.257	0.356	0.257	0.244	83.5	12.4	1.06
0.5	0.252	33.2	0.214	0.300	0.214	0.200	82.8	9.39	0.53
0.4	0.201	22.7	0.169	0.241	0.169	0.159	82.0	6.92	0.22
0.3	0.154	17.0	0.128	0.184	0.124	0.116	80.0	4.16	0.071
0.2	0.103	9.1	0.082	0.125	0.082	0.075	78.5	1.56	0.0159
0.1	0.055	2.3	0.040	0.076	0.040	0.024	64.0	0.32	0.00041

Here V_{IH} and V_{IL} are the input voltages HIGH and LOW at the operation points of $\frac{\partial V_{out}}{\partial V_{in}} = 1$ at the voltage transfer characteristics of the inverter, high and low noise margins (NM_H and NM_L) defined as $NM_H = V_{DD} - V_{IH}$, $NM_L = V_{IL}$, and total $NM = NM_H + NM_L$. The NM is expressed as a percentage of V_{DD}.

Reference

1. Yohannes, T. *et al.* Multiple electrochemical doping-induced insulator-to-conductor transitions observed in the conjugated ladder polymer polybenzimidazobenzophenanthroline (BBL). *J. Phys. Chem. B* **104**, 9430–9437 (2000).

2. Fazzi, D., Fabiano, S., Ruoko, T. P., Meerholz, K. & Negri, F. Polarons in π-conjugated ladder-type polymers: A broken symmetry density functional description. *J. Mater. Chem. C* **7**, 12876–12885 (2019).

3. Yin, J., Wang, Z., Fazzi, D., Shen, Z. & Soci, C. First-Principles Study of the Nuclear Dynamics of Doped Conjugated Polymers. *J. Phys. Chem. C* **120**, 1994–2001 (2016).

4. Cowan, S. R., Roy, A. & Heeger, A. J. Recombination in polymer-fullerene bulk heterojunction solar cells. *Phys. Rev. B - Condens. Matter Mater. Phys.* **82**, 245207 (2010).

5. Yao, J. *et al.* Cathode engineering with perylene-diimide interlayer enabling over 17% efficiency single-junction organic solar cells. *Nat. Commun.* **11**, 1–10 (2020).

6. Nikolka, M. *et al.* High operational and environmental stability of high-mobility conjugated polymer field-effect transistors through the use of molecular additives. *Nat. Mater.* **16**, 356–362 (2017).

7. Ponder, J. F. J., Österholm, A. M. & Reynolds, J. R. Conjugated Polyelectrolytes as Water Processable Precursors to Aqueous Compatible Redox Active Polymers for Diverse Applications: Electrochromism, Charge Storage, and Biocompatible Organic Electronics. *Chem. Mater.* **29**, 4385–4392 (2017).

8. Shi, P., Amb, C. M., Dyer, A. L. & Reynolds, J. R. Fast Switching Water Processable Electrochromic Polymers. *ACS Appl. Mater. Interfaces* **4**, 6512–6521 (2012).